Exploring in Extremely Dark: Low-Light Video Enhancement with Real Events

Anonymous Authors

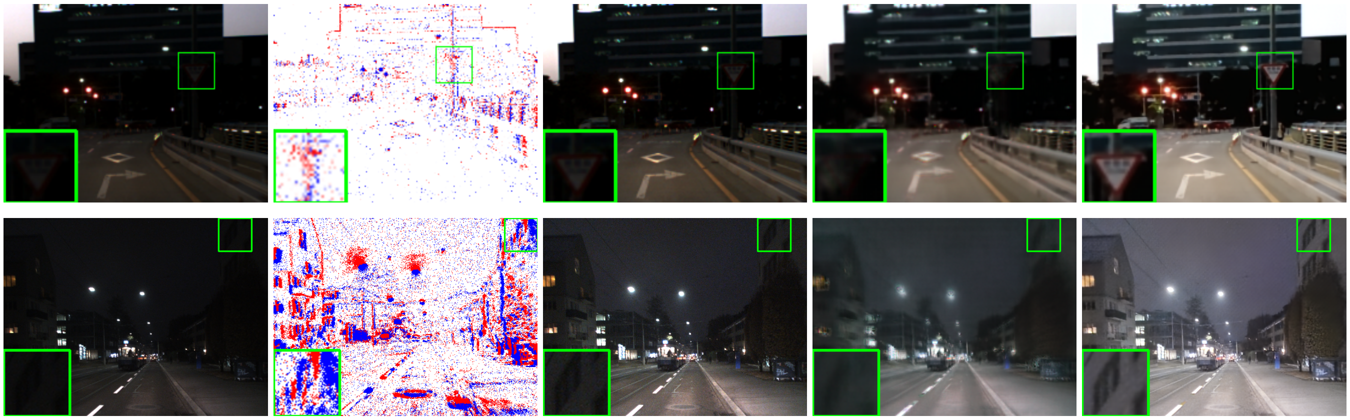

(a) Low-light Frames (b) Events (c) CLIP-LIT [17] (d) LAN [4] (e) REN

Figure 1: Given inputs of (a) low-light frames and (b) events, the normal-light frames can be enhanced using different methods shown in (c) CLIP-LIT (ICCV2023) [17], (d) LAN (ICCV2023) [4] and (e) the Real-Event Embedded Network (REN). These examples are tested on real data containing extremely dark regions. The REN is able to generate normal-light frames with more details and improved brightness.

ABSTRACT

Due to the limitations of sensor, traditional cameras struggle to capture details within extremely dark areas of videos. The absence of such details can significantly impact the effectiveness of low-light video enhancement. In contrast, event cameras offer a visual representation with higher dynamic range, facilitating the capture of motion information even in exceptionally dark conditions. Motivated by this advantage, we propose the Real-Event Embedded Network for low-light video enhancement. To better utilize events for enhancing extremely dark regions, we propose an Event-Image Fusion module, which can identify these dark regions and enhance them significantly. To ensure temporal stability of the video and restore details within extremely dark areas, we design unsupervised temporal consistency loss and detail contrast loss. Alongside the supervised loss, these loss functions collectively contribute to the semi-supervised training of the network on unpaired real data. Experimental results on synthetic and real data demonstrate the superiority of the proposed method compared to the state-of-the-art methods. Our codes will be publicly available.

ACM MM, 2024, Melbourne, Australia

ACM ISBN 978-x-xxxx-xxxx-x/YY/MM
https://doi.org/10.1145/nnnnnnn.nnnnnnn

CCS CONCEPTS

• **Computing methodologies** → **Neural networks**; **Machine learning algorithms**; **Reconstruction**; **Image Processing**.

KEYWORDS

Low-Light, Video Enhancement, Real Event, Extremely Dark

1 INTRODUCTION

Low-light video enhancement is a critical task in the field of computer vision, which aims to enhance the visibility and visual quality of videos captured under low-light conditions. Due to the constraints of low-light environments and the limitations of camera sensor, these videos often suffer from noticeable noise, insufficient information and blurriness, leading to the loss of details and a decrease in the overall quality. Despite significant progress in this field, low-light video enhancement remains a formidable challenge.

Many deep learning methods [1, 4, 11, 21, 34, 43] have been proposed to enhance low-light videos. However, most of these approaches rely on mining information directly from a video to enhance it. Due to the limitations of cameras, details in extremely dark areas of the videos are inevitably lost and remain missing even after the enhancement.

Event camera is an emerging sensor characterized by its large dynamic range and rapid response. Events recorded alongside low-light videos, even in extremely dark areas, can fully capture motion information, which is lacking in traditional cameras. This feature makes event cameras highly suitable for low-light video enhancement.

However, employing event cameras for low-light video enhancement faces several distinct challenges: 1) Fusion complexities: The information in the extremely dark regions of the video is limited, making it challenging to fuse event data with these areas and achieve effective enhancement. 2) Data acquisition difficulties: Constructing a dataset consisting of paired real events, normal-light videos and low-light videos is difficult. Most existing video-event paired datasets [6, 14] only consist one type of videos while also suffering from alignment issues. While event simulators [10, 27] can be used to generate synthetic events, the inherent disparities between synthetic and genuine data can compromise the inferential performance on real data.

In this paper, we propose the **R**eal-Event **E**mbedded **N**etwork (REN), a low-light video enhancement model that integrates event data based on the Retinex [13] theory. We tackle the challenges by the following strategies: To effectively fuse misaligned real events and images, we present Event-Image Fusion (EIF) module. It can adaptively identify extremely dark regions and utilize event information to enhance them. Furthermore, EIF module establishes spatial alignment between misaligned image and event features. To address the challenge of lacking genuine paired data, we propose unsupervised temporal consistency loss and detail contrast loss, which offer supervision at both temporal and spatial levels. They ensure the temporal consistency of input and output sequence, and spatially supervise detail reconstruction in extremely dark regions respectively. Together with the supervised loss, these loss functions collectively contribute to the semi-supervised training of the REN. The overall network is trained end-to-end with partially labeled datasets, which consist of paired low-light and normal-light videos with synthetic events, as well as solely low-light videos alongside real events.

In summary, the contributions of our work are as follows:

- We propose the Real-Event Embedded Network to leverage real events for addressing low-light enhancement challenges. To the best of our knowledge, it is the first exploration of real events in this field.
- We propose the Event-Image Fusion module, which can identify extremely dark regions and utilize event to enhance them.
- We design unsupervised temporal consistency loss and detail contrast loss, aiming to maintain temporal stability of videos and restore details in extremely dark regions.
- Extensive experiments on both real and synthetic datasets demonstrate that our approach outperforms state-of-the-art methods in low-light video and image enhancement.

2 RELATED WORK

Low-Light Video Enhancement This line of work primarily includes direct enhancement and Retinex-based enhancement. In the former, Liu et al. [18] employ neural networks to simulate event information from videos and fuse them. Zhang et al. [40] extract optical flow from individual images to enforce the temporal stability. Chhirolya et al. [2] propose a self-cross dilated attention module to learn inter-frame relationships in static videos. SGLLIE [43] extracts enhancement factors and recursively enhances videos. MBLLEN [21] and SMOID [11] employ 3D convolutions to harness the temporal information within videos. As for the Retinex-based enhancement, LAN [4] and SDSDNet [34] extract illumination from videos and enhance them, with LAN designing an adaptive brightness enhancement method capable of achieving one-to-multiple enhancement. In contrast to previous Retinex-based approaches, our focus lies on the reflectance, using event data to complement missing information in extremely dark regions.

Event-Based Video Reconstruction Event cameras have found widespread applications in the field of image and video reconstruction, including super-resolution [8, 20], high dynamic range [25, 39], deblurring [30, 36] and video frame interpolation [12, 31]. Considering the distinct modalities of image and event features, these works primarily focus on the fusion. In addition to simply summing or concatenating events and images [26, 33], HDRev [39] propose a multimodal representation alignment strategy to learn a shared latent space and a fusion module tailored to complement two types of signals in different regions. EvIntSR [8] constructs latent frames separately from events and images, followed by their fusion. EFNet [29] propose an Event-Image Cross-modal Attention fusion module, which allows attending to the event features via a channel-level attention mechanism. Very recently, Liang et al. [16] propose a low-light video enhancement method with hybrid inputs of events and frames, using synthetic events to train their network. The differences between these methods and our work are: 1) We employ real event for low-light video enhancement; 2) Our work focuses on enhancing extremely dark regions using event data, while other approaches treat all regions uniformly; 3) Our approach can deal with the misalignment image and event features through spatial-level attention.

3 PROPOSED METHOD

3.1 Formulation

Event Representation An event data $e = (p, t, \sigma)$ is triggered at time t and at pixel $p = (x, y)$ when the log intensity change ΔL between t and $t - \delta t$ exceeds the dispatched threshold θ, $\sigma \in \{+1, -1\}$ is the polarity that indicates the increase or decrease of intensity changes.

$$\Delta L = \| \log R_t^{(p)} - \log R_{t-\delta t}^{(p)} \| \tag{1}$$

where $R_t^{(p)}$ denotes the instantaneous intensity at time t and pixel p.

As event streams are sparse points and can not input into network, we represent the events as 3D voxel grid [44]. By discretizing duration $\Delta t = t_{K-1} - t_0$ spanned by K events into C temporal bins, each event $e_k = (p_k, t_k, \sigma_k)$ distributes its polarity σ_k to the two closest voxels:

$$E_t^{(p)} = \sum_{p_k = p} \sigma_k \max(0, 1 - \mid t - \widetilde{t_k} \mid) \tag{2}$$

where $\widetilde{t_k} = \frac{C-1}{\Delta t}(t_k - t_0)$ is the normalized timestamp.

Problem Statement Classic Retinex-based model assumes that image can be decomposed into reflectance and illumination, similar to [3], we employ a regularization-free method to represent the image I:

$$I = \phi_s(\phi_R(I), \phi_L(I)) \tag{3}$$

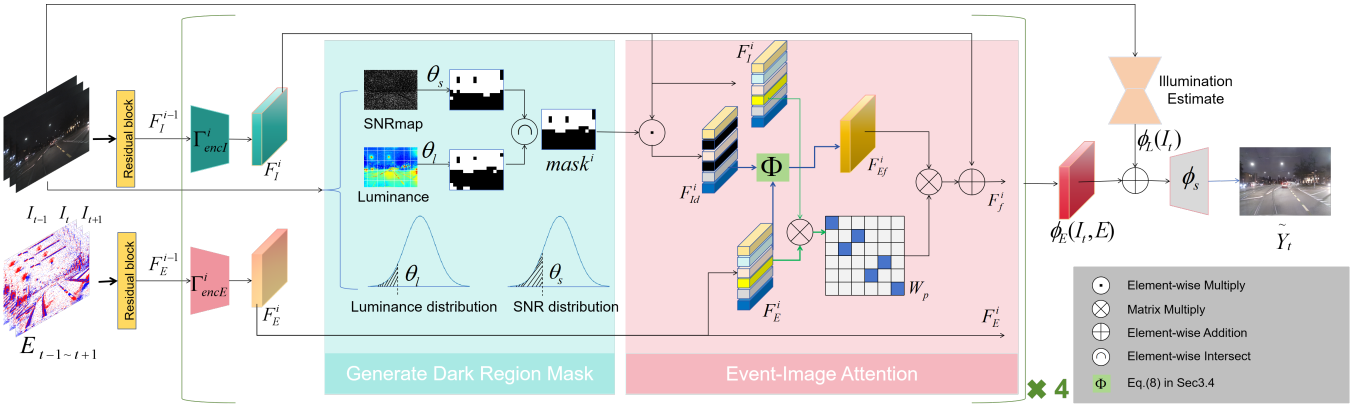

Figure 2: An overview of the proposed REN. Based on the Retinex theory, estimate the illumination and reflection of input frames. Generate Dark Region Mask to identify the extremely dark regions, then fuse event and image features to enhance the reflection in these regions using the Event-Image Attention module. Finally, merge the illumination and reflection to obtain the enhanced frame.

where ϕ_R, ϕ_L denote the modules used to estimate reflectance and illumination respectively, and ϕ_s denotes the module used to synthesize the reflectance and illumination.

Previous methods primarily focus on accurately estimating these two components and their fusion, often directly assuming the estimated reflectance is same as the ground truth [3, 4]. However, in extremely dark regions, the reflectance tends to lack fine details, owing to the limitations of conventional camera sensors. Different from prior work, our approach enhances the reflectance using event data, the enhanced image $\widetilde{Y_t}$ can be defined as:

$$\widetilde{Y_t} = \phi_s(\phi_E(I_l, E), \phi_L(I_l)) \tag{4}$$

and the objective function is as follows:

$$\begin{aligned} \min_{\phi_s,\phi_L,\phi_E} \; & \| I_n - \phi_s(\phi_E(I_l, E), \phi_L(I_l)) \|_F^2 + \\ & \| \phi_R(I_n) - \phi_E(I_l, E) \|_F^2 \end{aligned} \tag{5}$$

where I_n, I_l and E denote normal-light image, low-light image and event respectively; ϕ_E denotes the reflectance estimated from events and images; and $\| \cdot \|_F$ represents the Frobenius norm.

3.2 General Architecture of REN

Fig. 2 illustrates the overall architecture of the proposed REN. Given input video frames $I_{t+j,j\in[-k,k]}$ and an event sequence $E_{t-k\sim t+k}$, we first concatenate and project them as embedding $F_I^{(0)} \in R^{H\times W\times C}$ and $F_E^{(0)} \in R^{H\times W\times C}$ respectively through a Residual Block [9]. Then we estimate the reflectance $\phi_E(I_t, E)$ and illumination $\phi_L(I_t)$ from them, and finally synthesize them into normal light frames $\widetilde{Y_t}$.

We use a dual-branch structure to estimate the reflectance $\phi_E(I_t, E)$, with a branch dedicated to extract image features and the other to extract the event features respectively. Every branch is structured as a hierarchy with four stages. Each stage of the image branch consists of an image encoder Γ_I^i and an Event-Image Fusion module (EIF, will be detailed in Sec. 3.3). Each stage of event branch only consists of an event encoder Γ_E^i. For the i-th stage, the image feature $F_I^{i-1} \in R^{\frac{H}{2^{i-1}}\times\frac{W}{2^{i-1}}\times 2^{i-1}C}$ and event feature $F_E^{i-1} \in R^{\frac{H}{2^{i-1}}\times\frac{W}{2^{i-1}}\times 2^{i-1}C}$ will first be processed as $F_I^i \in R^{\frac{H}{2^i}\times\frac{W}{2^i}\times 2^iC}$ and $F_E^i \in R^{\frac{H}{2^i}\times\frac{W}{2^i}\times 2^iC}$ through image encoder Γ_I^i and event encoder Γ_E^i respectively. Then these features are jointly fed into the EIF module to obtain the fused features $F_f^i \in R^{\frac{H}{2^i}\times\frac{W}{2^i}\times 2^iC}$, we set $F_I^i = F_f^i$ as the input for the next stage. F_f^4 will be considered as the reflectance $\phi_E(I_t, E)$.

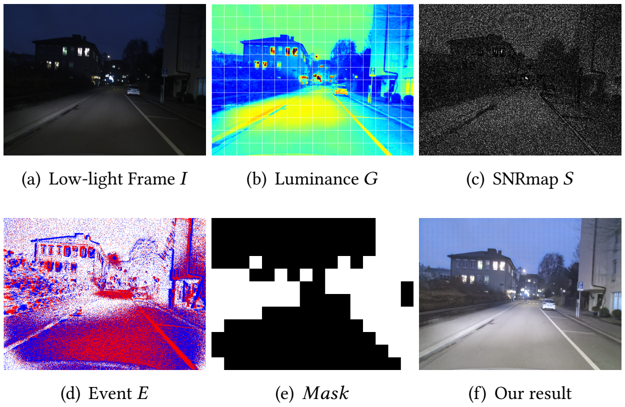
(a) Low-light Frame I (b) Luminance G (c) SNRmap S

(d) Event E (e) *Mask* (f) Our result

Figure 3: Visualization of the Luminance (b) and SNRmap (c) extracted from input frame (a). The extremely dark regions mask is (e), the input events is (d) and our result is (f).

Considering that the illumination requires more global features, we first encode $F_I^{(0)}$ into the latent space, followed by a U-Net [28] to estimate the Illumination $\phi_L(I_t)$.

The estimated illumination $\phi_L(I_t)$ and reflectance $\phi_E(I_t, E)$ are first aligned by convolutional layers, after which the aligned features are fed into the decoder ϕ_s to synthesize them. In addition, we also employ residual connections between image encoders and the decoder to improve the performance. In the end, the output of the decoder is processed through a convolutional layer to obtain the enhanced frame $\widetilde{Y_t}$.

3.3 Event-Image Fusion

The fusion of image features and event features is the key to event-based low-light enhancement, requiring the matching of relevant features from both the image and the event. Due to the limited information in the ultra-dark regions and interference from other areas, matching is very challenging.

Generate Dark Region Mask We design a patch-based extremely dark region mask to identify these regions, so the constraints imposed by the two conditions mentioned above can be relaxed when matching with events. As the extremely dark regions are included in the patch, information within the patch can be used for matching with event features, reducing the difficulty of matching, meanwhile avoiding interference from information outside the patch.

Due to the extremely low brightness and Signal-to-Noise Ratio (SNR) in the ultra-dark regions, we use SNR distribution and luminance distribution to generate the mask. We calculate the SNR map using the method similar to [37], and regard the grayscale image as luminance map. Specifically, given the frames $I_{t+j,j\in[-k,k]}$, we calculate the luminance map G and SNR map S of I_t, and then count their distribution.

$$\begin{aligned} G &= Gray(I_t) \\ \widetilde{I_t^g} &= denoise(Gray(I_t)) \\ S &= \frac{\widetilde{I_t^g}}{abs(I_t^g - \widetilde{I_t^g})} \end{aligned} \tag{6}$$

where $Gray$ denotes the process of obtaining a grayscale image, $denoise$ represents a non-learning-based denoising operation. For the i-th stage, $F_I^i \in R^{h\times w\times c}$, we first resize G and S to (h, w), then divide them into non-overlapping patches $G_{j,j\in[1,2,\ldots,m]}$ and $S_{j,j\in[1,2,\ldots,m]}$, using a window of size (ws, ws). Then $mask^i$ is get through:

$$mask_j^i = \begin{cases} 1, & mean(G_j) < \theta_l \& mean(S_j) < \theta_s \\ 0, & else \end{cases} \tag{7}$$

where $mean$ denotes taking the average value, $mask_j^i$ denotes the j-th patch of $mask^i$, θ_l and θ_s are thresholds based on luminance distribution and SNR distribution respectively. We set θ_l and θ_s as the last 10% of luminance distribution and the last 30% of SNR distribution respectively. The extremely dark region feature of images can be defined as $F_{Id}^i = F_I^i \times mask^i$.

Difference from previous mask-based method [37], we integrate both luminance and SNR rather than solely focusing on one, and employ adaptive thresholds, which grant it superior generalization capability. Additionally, our mask operates at the patch level rather than the pixel level, which contributes more effectively to the fusion of images and events.

Event-Image Attention Most real datasets suffer from alignment issues between videos and events, we utilize a novel Event-Image Attention fusion to fuse them, and establish spatial mapping relationships to faciliate the alignment. Specifically, given the image feature $F_I^i \in R^{h\times w\times c}$, dark regions feature $F_{Id}^i \in R^{h\times w\times c}$ and event feature $F_E^i \in R^{h\times w\times c}$, we use 1×1 conv to get queries Q_{id} from F_{Id}^i, Q_i from F_I^i, keys K_e and values V_e from F_E^i respectively. Then we divide them into patches using a window of size (ws, ws). The shape of features are changed from (c, h, w) to $(h/ws\times w/ws, ws\times ws\times c)$, where each patch represents features from different spatial positions. The aggregated event feature F_{Ef}^i is written as:

$$F_{Ef}^i = \Phi(Q_{id}, K_e, V_e) = V_e Softmax(\frac{Q_{id}^T K_e}{\sqrt{d_k}}), \tag{8}$$

d_k denotes the dimension of the features. It makes event feature focusing on extremely dark areas. To establish the spatial mapping relationship, we calculate an attention similarity between F_I^i and F_E^i:

$$W_p = Q_i^T K_e \tag{9}$$

which serves as a measure of the similarity between every image patch and event patch. For misaligned image and event features, we consider an event patch with the highest similarity to an image patch to be one that matches the image patch. Consequently, we set the maximum value of each row in W_p to 1 while the remaining values to 0, and utilize it to establish a spatial mapping between two types of patches via:

$$\widetilde{F_{Ef}^i} = W_p^T F_{Ef}^i \tag{10}$$

where $\widetilde{F_{Ef}^i}$ represents the event features aligned with the image features. Finally, the output of EIF is:

$$F_f^i = \widetilde{F_{Ef}^i} + F_I^i \tag{11}$$

3.4 Temporal Consistency Loss

An event stream $E_{t-\Delta t\sim t+\Delta t}$ records dynamic information between $t-\Delta t$ and $t+\Delta t$. When $\Delta t \to 0$, it indicates a very small motion and reflects the motion trend. To better keep the temporal stability of output frames, we design the temporal consistency Loss L_t, which estimates the motion trend at time t from frame I_t and compares it with the input. For the synthetic data, the input events are aligned with the frames, and the temporal consistency loss is:

$$L_t^s = \| v(\widetilde{Y_t}) - E_{t-\Delta t\sim t+\Delta t} \|_F^2, \Delta t \to 0 \tag{12}$$

For the real data, the input events and the frames are misaligned, the temporal consistency loss is:

$$L_t^r = \| v(I_t) - v(\widetilde{Y_t}) \|_F^2 \tag{13}$$

where v denotes a U-Net [28] structure used to extract motion trend from frames.

3.5 Detail Contrast Loss

The detailed information in extremely dark areas is lost while relatively complete in other areas. To restore complete details in the enhanced frame, we encourage greater discrepancies between input frames and output frames in extremely dark regions, while reducing discrepancies in other areas. The loss function is defined as follows:

$$L_{con} = \frac{\| (I_t - \widetilde{Y_t})(1 - mask) \|_F^2}{\| (I_t - \widetilde{Y_t})(1 - mask) \|_F^2 + \| (I_t - \widetilde{Y_t})mask \|_F^2} \tag{14}$$

where $mask$ identifies the extremely dark region.

Furthermore, we also employ the L_{clip} in [17] to preserve the semantic integrity of the enhanced results.

$$L_{clip} = \frac{e^{cos(\Phi_{image}(\widetilde{Y_t}),\Phi_{text}(T_n))}}{\sum_{i\in\{n,p\}} e^{cos(\Phi_{image}(\widetilde{Y_t}),\Phi_{text}(T_i))}} + w\cdot \parallel \Phi_{image}(\widetilde{Y_t}) - \Phi^{l}_{image}(I_t) \parallel_2 \quad (15)$$

where Φ_{image} and Φ_{text} denote the image encoder and text encoder in CLIP model respectively, w is the weight. We set T_n = "normal light image" and T_p = "low light image".

3.6 Optimization

We propose to train the REN over a partially labeled dataset, composed of the synthetic dataset D_s with groundtruth and the real dataset D_r without groundtruth. We employ L^s_t, L_{error} for D_s, and L^r_t, L_{con}, L_{clip} for D_r. L_{error} is the reconstruction loss according to Eq. 5:

$$L_{error} = \parallel \widetilde{Y_t} - I_n \parallel^2_F + \parallel \phi_E(I_n, E) - \phi_E(\widetilde{Y_t}, E) \parallel^2_F \quad (16)$$

Thus the overall function is as follows:

$$L = L_{error} + \alpha L^s_t + \beta L^r_t + \gamma L_{con} + \delta L_{clip} \quad (17)$$

where α, β, γ and δ denote the balancing parameters.

4 EXPERIMENTS

4.1 Experimental Settings

Dataset The proposed Real-Event Embedded Network is trained in a semi-supervised strategy, where one synthetic dataset (SDSD dataset [34]) is provided for training with the groundtruth and one real dataset (DSEC dataset [6]) for unsupervised training. In addition, we use the ViViD++ dataset [14, 15] for cross-dataset evaluation.

SDSD: Based on the SDSD dataset [34], we build a syntheic dataset composed of synthetic events as well as real low-light videos and normal-light videos. We employ V2E [10] to simulate events from low-light videos. The detailed configuration of V2E can be found in the **supplementary material**.

DSEC: DSEC dataset [6] consists of real videos and events captured by Prophesee Gen3.1M camera. We select low-light videos along with events from it to train and test our method. We choose 10 training videos with a total of 2948 frames, along with 19 test videos totaling 570 frames.

ViViD++: Similar to the DSEC dataset, ViViD++ dataset consists of real videos and events captured by DVXplorer camera. We select low-light videos along with events from it for cross-dataset evaluation. Due to ViViD++ is collected from real-world scenarios, it reflects the effectiveness of the method in real-world settings.

Implementation Details Our network is implemented using Pytorch on NVIDIA Geforce RTX 3090. During training, we randomly crop the samples into 320 × 320 patches and augment the data using rotation and horizontal flipping. We optimize the network by AdamW optimizer [19] with the momentum terms of (0.9, 0.999). We set the learning rate to 4e-4 and use the cosine decay strategy to decrease it. The total epoch of training is set to 100 and the balancing parameters α, β, γ, δ and w are all set to 1. To validate the effectiveness of exploiting real event, REN is trained respectively over two different datasets: SDSD and SDSD + DSEC, and final networks are respectively denoted as REN$_{sd}$ and REN. Specifically, REN$_{sd}$ is trained only over syntheic SDSD dataset, while REN is trained over syntheic SDSD dataset and real DSEC dataset.

4.2 Quantitative Evaluation

To comprehensively evaluate the effectiveness of our proposed method, we compare REN with SOTA methods using the SDSD dataset and DSEC dataset.

Evaluation on SDSD dataset. We train and test the SOTA methods on SDSD dataset for quantitative evaluations, the testset of SDSD dataset includes 12 indoor video pairs and 13 outdoor video pairs.

We adopt three evaluation metrics: Peak Singal-to-Noise Ratio (PSNR), Structural Similarity (SSIM) [35] and Learned Perceptual Image Patch Similarity (LPIPS) [42]. PSNR quantifies image quality by comparing signal power to noise. SSIM assesses the image similarity by considering luminance, contrast and structure. LPIPS measures the perceptual image patch similarity using deep learning.

The results are shown in Table 1, the $*$ in table means unsupervised methods. As these methods can be trained on SDSD dataset or SDSD+DSEC datasets, which is similar to ours, we only present the best results of these methods in the table, and the full results are presented in the **supplementary materials**. As shown in the table, REN$_{sd}$ outperforms all supervised methods and REN achieves the best performance. Furthermore, the application of real events and our semi-supervised training strategy is shown to be very effective in improving the performance of the model.

Evaluation on DSEC dataset. We also compare different methods on the DSEC real dataset. For supervised methods, due to the lack of groundtruth in the DSEC dataset, it is not feasible to them. Therefore, to compare them with our method, we generate results using models trained on the SDSD dataset, which is consistent with the REN$_{sd}$. For the unsupervised methods (marked with $*$), we train them on SDSD+DSEC datasets and compare them with REN.

We employ four no-reference evaluation metrics: Natural Image Quality Evaluator (NIQE) [24], Integrated Local NIQE (ILNIQE) [41], Perceptual Index (PI) [22] and Perception based Image Quality Evaluator (PIQE) [32]. NIQE assesses the image naturalness based on statistical properties. ILNIQE is an opinion-unaware blind image quality assessment method. PI evaluates the image quality based on human perceptual assessment. PIQE is based on the perceptual characteristics of the human visual system. The evaluation results are shown in Table 2, under the same training dataset conditions, REN$_{sd}$ outperforms all supervised methods, while REN outperforms all unsupervised methods among all the metrics.

We also integrate event to two recently best low-light video enhancement methods, SDSDNet [34] and LAN [4], for a more fair comparison. They are represented as SDSDNet + Event and LAN + Event respectively. Specifically, we incorporate the EIF module into them and train them on SDSD dataset. As shown in Table 3, both methods improve the performance after integrated with events, and our method achieves the best results.

4.3 Qualitative Evaluation

We perform qualitative assessments on the SDSD and DSEC datasets, and cross-dataset evaluations on ViViD++ dataset. Fig. 4 presents

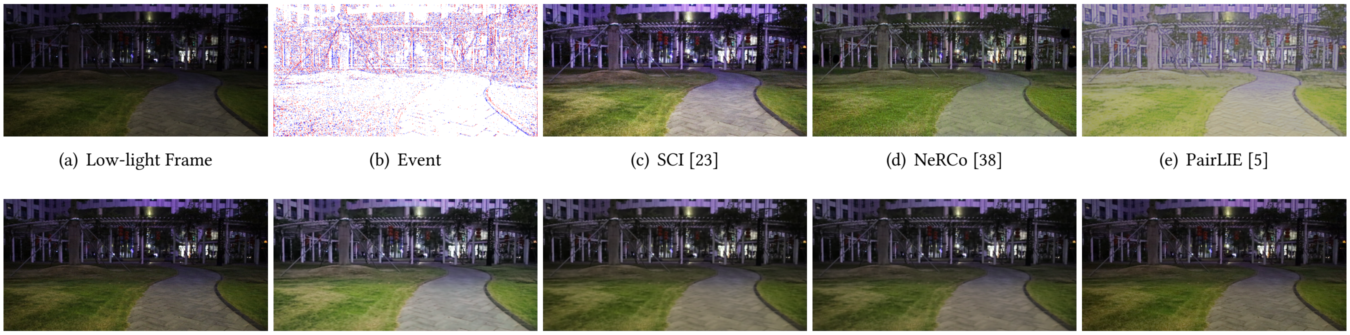

(a) Low-light Frame (b) Event (c) SCI [23] (d) NeRCo [38] (e) PairLIE [5]

(f) CLIP-LIT [17] (g) LAN [4] (h) REN$_{sd}$ (i) REN (j) GroundTruth

Figure 4: Visual quality comparison of enhancement results on SDSD synthetic dataset.

Table 1: Quantitative results of different methods on SDSD dataset, $*$ means unsupervised methods.

Methods	Learning	PSNR↑	SSIM↑	LPIPS↓
PairLIE [5]	Image	13.37	0.54	0.22
SCI* [7]	Image	19.67	0.69	0.29
SNR-Aware [37]	Image	25.28	0.82	0.13
NeRCo* [38]	Image	20.07	0.66	0.21
CLIP-LIT* [17]	Image	22.29	0.72	0.16
MBLLEN [21]	Video	21.79	0.65	0.19
SGLLIE* [43]	Video	23.89	0.70	0.31
SMID [1]	Video	24.09	0.69	0.21
SDSDNet [34]	Video	24.92	0.73	0.14
LAN [4]	Video	27.25	0.85	0.12
REN$_{sd}$	Video	28.45	**0.88**	**0.09**
REN	Video	**29.03**	**0.88**	**0.09**

Table 2: Quantitative results of different unsupervised methods on DSEC dataset, $*$ means unsupervised methods.

Methods	NIQE↓	ILNIQE↓	PI↓	PIQE↓
PairLIE [5]	12.08	33.66	3.80	20.59
SNR-Aware [37]	11.58	23.53	3.52	8.16
MBLLEN [21]	13.07	23.07	3.32	19.18
SMID [1]	20.89	26.88	9.10	13.22
SDSDNet [34]	14.16	34.93	5.64	15.47
LAN [4]	22.30	33.66	3.80	23.59
REN$_{sd}$	10.84	20.76	3.26	15.65
SCI* [23]	11.70	21.30	3.41	8.35
NeRCo* [38]	13.64	22.63	2.71	14.70
CLIP-LIT* [17]	10.42	22.89	3.43	9.64
SGLLIE* [43]	11.07	24.11	3.77	8.57
REN	**10.28**	**20.69**	**2.69**	**8.01**

Table 3: Quantitative results of two recently best low-light video enhancement methods integrated with event on SDSD dataset.

Methods	PSNR↑	SSIM↑	LPIPS↓
SDSDNet [34]	24.92	0.73	0.14
SDSDNet + Event	25.81	0.85	0.11
LAN [4]	27.25	0.85	0.12
LAN + Event	28.20	0.87	0.10
REN$_{sd}$	**28.45**	**0.88**	**0.09**

the results obtained on the SDSD dataset, similar to Table 1, we present the best results of unsupervised methods. In comparison to the groundtruth, the CLIP-LIT produces results with weak enhancement and low brightness. The PairLIE generates unrealistic outcomes. NeRCo, SCI and LAN suffer from significant color deviation, which adversely impairs the visual quality of the images.

Fig. 5 presents the visual results obtained on the DSEC dataset, which comprises low-quality videos with numerous extremely dark regions, posing a considerable challenge for enhancement. All the method are trained on SDSD+DSEC datasets. The SCI and CLIP-LIT result in significantly reduced brightness and severe noise, they are unable to effectively recover details in extremely dark areas. The result generated by NeRCo exhibits noticeable striping artifacts. The SGLLIE exhibits severe white noise and generates unrealistic results. Due to training exclusively on synthetic dataset, REN$_{sd}$ exhibits issues of insufficient brightness and unclear details on real data. In contrast, REN is trained on real data and demonstrates favorable results in enhancing details, improving brightness, and mitigating noise in extremely dark regions.

Fig. 6 shows the visual results obtained on the ViViD++ dataset. These results are generated using the models presented in Table 2. The PairLIE enhances the brightness but generates unrealistic color tones. The images enhanced by NeRCo and SDSDNet exhibit noticeable artifacts. CLIP-LIT and SCI fail to enhance the brightness adequately, while the result enhanced by LAN appears relatively blurry. The image enhanced by REN$_{sd}$ lacks sufficient clarity and exhibits blurriness in the details. In contrast, REN generates more realistic and clearer result.

Fig. 7 shows the visual results of SDSDNet and LAN as well as their integration with event, it also shows the result of our method. Upon the integration with event, both SDSDNet and LAN exhibit noticeable improvements in detail recovery and visual effects, demonstrating the efficacy of event and EIF module. Meanwhile, REN$_{sd}$ and REN achieve the most favorable visual results.

After a comprehensive evaluation of the comparative results of various methods across the three datasets, our proposed approach demonstrates outstanding visual performance in global brightness and detail restoration. More experimental results can be found in the **supplementary material**.

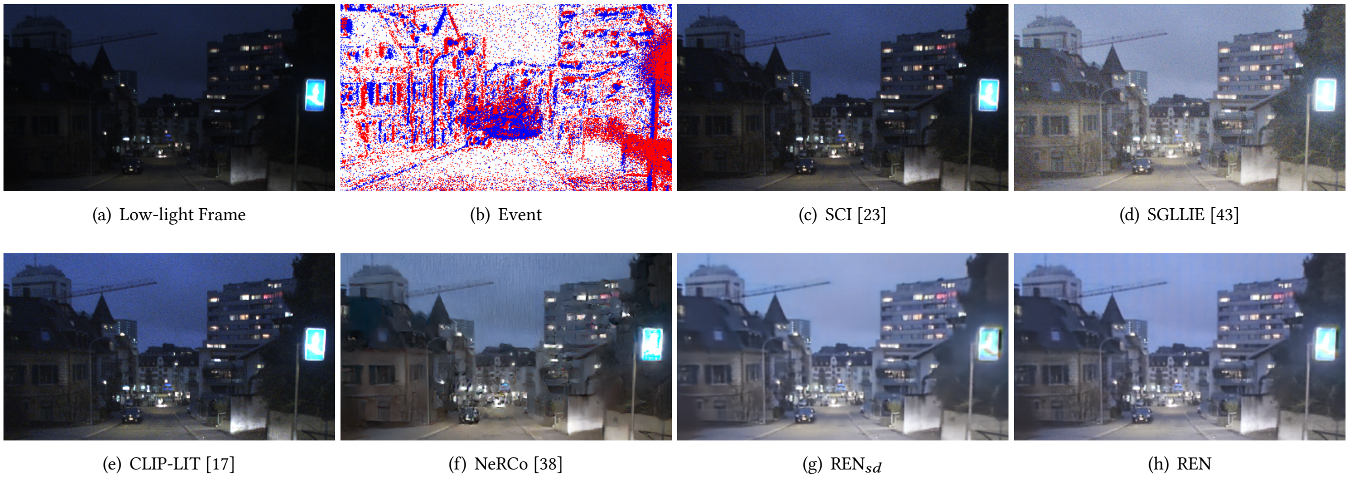

Figure 5: Visual quality comparison of enhancement results on DSEC real dataset.

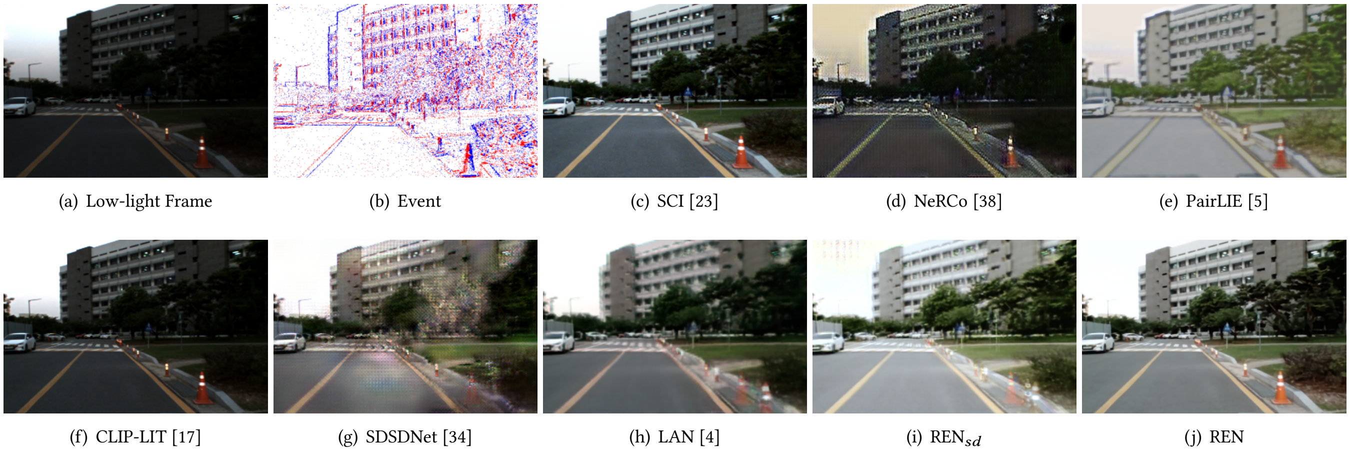

Figure 6: Visual quality comparison of enhancement results on ViViD++ real dataset.

4.4 Ablation Study

The proposed REN improves the performance of low-light video enhancement. To find out what contributes to the remarkable effectiveness of our approach, we do an ablation study and show the results in Table 4 and Fig. 8.

The effectiveness of Events. To validate the effectiveness of events, we train the model only using videos (Only Video). The PSNR value of this model decreases sharply by 2.91dB, which indicates the significant impact of events. As shown in Fig. 8, events significantly contribute to the recovery of details. The effectiveness of real events (REN$_{sd}$, W/o Real Events) is already demonstrated in Table 1 and Table 2, where REN outperforms REN$_{sd}$ on all datasets, and as shown in Fig. 8, REN achieves superio results on real data compared to REN$_{sd}$ (W/o Real Events).

The effectiveness of EIF Module. The EIF module consists of two parts, and concurrently establishes the mapping relationship between images and events, so we build three modified models for ablation study. 1) W/o Dark Region Mask (W/o DRM), which means we remove Dark Region Mask from the model. 2) W/o Event Image Attention (W/o EIA), which means we replace the Event Image Attention with a U-Net, as Dark Region Mask is designed to complement Event Image Attention, we also remove it. 3) W/o W_p, which means we remove W_p and Eq. 10 from EIF Module, rendering it incapable of establishing spatial alignment between images and

Table 4: Quantitative results of ablation study on SDSD testset.

Model	PSNR↑	SSIM↑	LPIPS↓
Only Video	26.12	0.86	0.10
REN$_{sd}$ (W/o Real Events)	28.45	0.88	0.09
W/o DRM	27.15	0.87	0.11
W/o EIA	26.29	0.87	0.09
W/o W_p	27.63	0.87	0.09
W/o L_t and L_{con}	28.61	0.88	0.09
W/o L_t	28.80	0.88	0.09
W/o L_{con}	28.91	0.88	0.09
REN	**29.03**	0.88	0.09

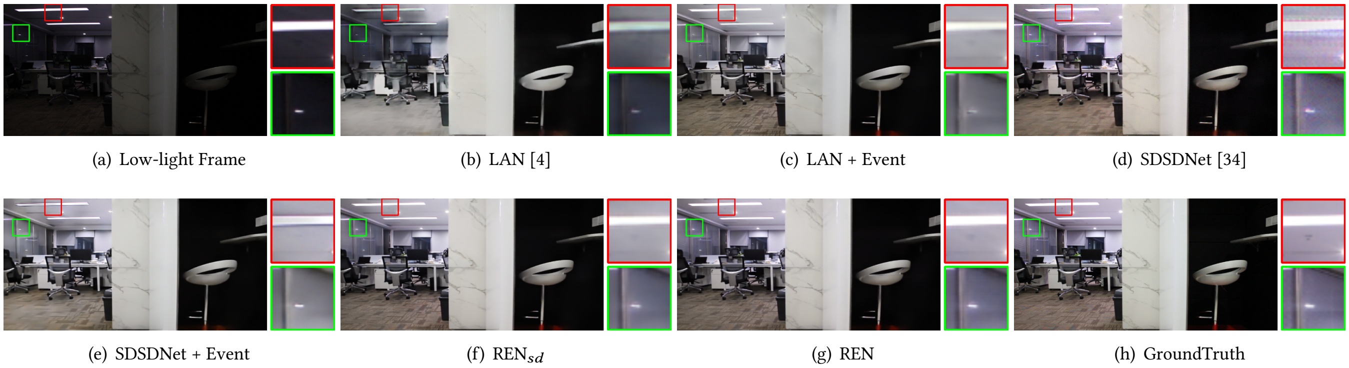
(a) Low-light Frame (b) LAN [4] (c) LAN + Event (d) SDSDNet [34]

(e) SDSDNet + Event (f) REN$_{sd}$ (g) REN (h) GroundTruth

Figure 7: Visual results of SDSDNet [34] and LAN [4] as well as their integration with event.

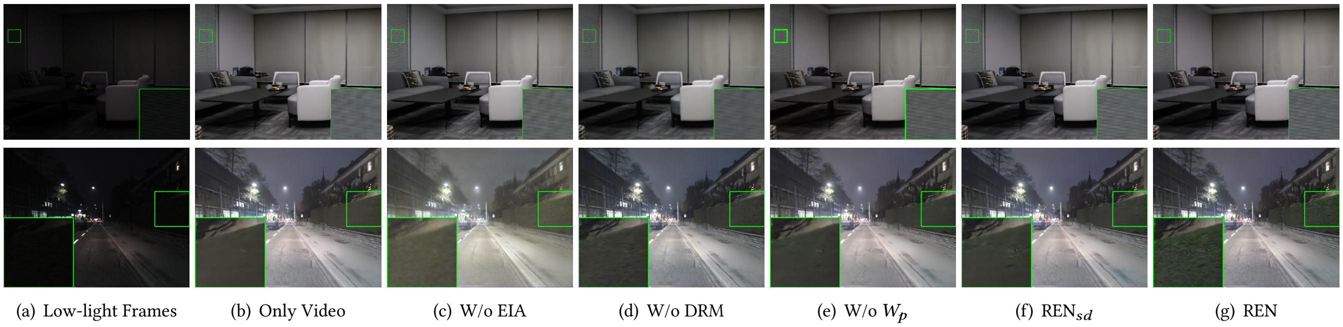
(a) Low-light Frames (b) Only Video (c) W/o EIA (d) W/o DRM (e) W/o W_p (f) REN$_{sd}$ (g) REN

Figure 8: Visual result of our ablation study. The top row is synthetic data from SDSD dataset and the bottom row is real data from DSEC dataset.

Table 5: The results of the user study. "REN" means that our result is preferred, "Other" means some other approach is preferred, "Same" means that the users have no preference.

Methods	Other	Same	REN
MBLLEN [21]	15%	5%	80%
SGLLIE [43]	5%	0%	95%
SMID [1]	0%	0%	100%
SDSDNet [34]	5%	5%	90%
LAN [4]	15%	25%	60%

events. The PSNR value of these models drop 1.88dB, 2.74dB and 1.4dB respectively. As shown in Fig. 8, the models W/o DRM and W/o EIA demonstrate unsatisfactory performance in the recovery of details within extremely dark regions. Due to the inability to align with real events and images, the model W/o W_p fails to fully leverage event information and recover details on real data. The result shows the effectiveness of our EIF module. More detailed discussions regarding the network architecture can be found in the **supplementary material**.

The effectiveness of temporal consistency loss and detail contrast loss. To validate the effectiveness of the proposed L_t and L_{con}, we build three modified strategies: 1) W/o L_t and L_{con}, which means training the model only using L_{clip} and L_{error}. 2) W/o L_t, which means training the model without L_t. 3) W/o L_{con}, which means training the model without L_{con}. The PSNR value of these models drop 0.42dB, 0.23dB, 0.12dB respectively, which shows the effectiveness of our proposed L_t and L_{con}.

4.5 User Study

We conduct user studies with 20 participants to compare the subjective visual quality of REN and other low-light video enhancement methods, including MBLLEN [21], SGLLIE [43], SMID [1], SDSDNet [34], LAN [4]. We randomly select 10 enhanced videos from the enhancement results of ViViD++ [14, 15] dataset to compare the performance of different models.

Each participant underwent five sets of test. In each set, participants are required to randomly select one method from the five options excluding REN and then choose a video randomly. They are instructed to compare the enhancement results of the selected method with REN on that particular video, and then they should decide which is better. The quantitative results of the user studies are shown in Table 5, indicating that our method is more appealing to users compared to other approaches.

5 CONCLUSION

In this work, to address the issue of information loss in extremely dark regions on low-light video enhancement, we propose the Real-Event Embedded Network, which leverages events to enhance such regions in low-light videos. We also design unsupervised temporal consistency loss and detail contrast loss, aiming to maintain temporal stability of videos and restore details in extremely dark regions respectively. These two loss functions, along with the supervised loss, are jointly employed in a semi-supervised manner to train the network on real data. Extensive experiments demonstrate that our method achieves SOTA performance.

REFERENCES

[1] Chen Chen, Qifeng Chen, Minh N Do, and Vladlen Koltun. 2019. Seeing motion in the dark. In *Proceedings of the IEEE/CVF International conference on computer vision*. 3185–3194.

[2] Shivam Chhirolya, Sameer Malik, and Rajiv Soundararajan. 2022. Low Light Video Enhancement by Learning on Static Videos with Cross-Frame Attention. *arXiv preprint arXiv:2210.04290* (2022).

[3] Huiyuan Fu, Wenkai Zheng, Xiangyu Meng, Xin Wang, Chuanming Wang, and Huadong Ma. 2023. You Do Not Need Additional Priors or Regularizers in Retinex-Based Low-Light Image Enhancement. In *Proceedings of the IEEE/CVF Conference on Computer Vision and Pattern Recognition*. 18125–18134.

[4] Huiyuan Fu, Wenkai Zheng, Xicong Wang, Jiaxuan Wang, Heng Zhang, and Huadong Ma. 2023. Dancing in the Dark: A Benchmark towards General Low-light Video Enhancement. In *Proceedings of the IEEE/CVF International Conference on Computer Vision*. 12877–12886.

[5] Zhenqi Fu, Yan Yang, Xiaotong Tu, Yue Huang, Xinghao Ding, and Kai-Kuang Ma. 2023. Learning a Simple Low-Light Image Enhancer From Paired Low-Light Instances. In *Proceedings of the IEEE/CVF Conference on Computer Vision and Pattern Recognition*. 22252–22261.

[6] Mathias Gehrig, Willem Aarents, Daniel Gehrig, and Davide Scaramuzza. 2021. Dsec: A stereo event camera dataset for driving scenarios. *IEEE Robotics and Automation Letters* 6, 3 (2021), 4947–4954.

[7] Chunle Guo, Chongyi Li, Jichang Guo, Chen Change Loy, Junhui Hou, Sam Kwong, and Runmin Cong. 2020. Zero-reference deep curve estimation for low-light image enhancement. In *Proceedings of the IEEE/CVF conference on computer vision and pattern recognition*. 1780–1789.

[8] Jin Han, Yixin Yang, Chu Zhou, Chao Xu, and Boxin Shi. 2021. Evintsr-net: Event guided multiple latent frames reconstruction and super-resolution. In *Proceedings of the IEEE/CVF International Conference on Computer Vision*. 4882–4891.

[9] Kaiming He, Xiangyu Zhang, Shaoqing Ren, and Jian Sun. 2016. Deep residual learning for image recognition. In *Proceedings of the IEEE conference on computer vision and pattern recognition*. 770–778.

[10] Yuhuang Hu, Shih-Chii Liu, and Tobi Delbruck. 2021. v2e: From video frames to realistic DVS events. In *Proceedings of the IEEE/CVF Conference on Computer Vision and Pattern Recognition*. 1312–1321.

[11] Haiyang Jiang and Yinqiang Zheng. 2019. Learning to see moving objects in the dark. In *Proceedings of the IEEE/CVF International Conference on Computer Vision*. 7324–7333.

[12] Taewoo Kim, Yujeong Chae, Hyun-Kurl Jang, and Kuk-Jin Yoon. 2023. Event-Based Video Frame Interpolation With Cross-Modal Asymmetric Bidirectional Motion Fields. In *Proceedings of the IEEE/CVF Conference on Computer Vision and Pattern Recognition*. 18032–18042.

[13] Edwin H Land. 1977. The retinex theory of color vision. *Scientific american* 237, 6 (1977), 108–129.

[14] Alex Junho Lee, Younggun Cho, Young-sik Shin, Ayoung Kim, and Hyun Myung. 2022. ViViD++: Vision for visibility dataset. *IEEE Robotics and Automation Letters* 7, 3 (2022), 6282–6289.

[15] Alex Junho Lee, Younggun Cho, Sungho Yoon, Youngsik Shin, and Ayoung Kim. 2019. ViViD: Vision for visibility dataset. In *IEEE Int. Conf. Robotics and Automation (ICRA) Workshop: Dataset Generation and Benchmarking of SLAM Algorithms for Robotics and VR/AR*.

[16] Jinxiu Liang, Yixin Yang, Boyu Li, Peiqi Duan, Yong Xu, and Boxin Shi. 2023. Coherent Event Guided Low-Light Video Enhancement. In *Proceedings of the IEEE/CVF International Conference on Computer Vision*. 10615–10625.

[17] Zhexin Liang, Chongyi Li, Shangchen Zhou, Ruicheng Feng, and Chen Change Loy. 2023. Iterative prompt learning for unsupervised backlit image enhancement. In *Proceedings of the IEEE/CVF International Conference on Computer Vision*. 8094–8103.

[18] Lin Liu, Junfeng An, Jianzhuang Liu, Shanxin Yuan, Xiangyu Chen, Wengang Zhou, Houqiang Li, Yan Feng Wang, and Qi Tian. 2023. Low-light video enhancement with synthetic event guidance. In *Proceedings of the AAAI Conference on Artificial Intelligence*, Vol. 37. 1692–1700.

[19] Ilya Loshchilov and Frank Hutter. 2017. Decoupled weight decay regularization. *arXiv preprint arXiv:1711.05101* (2017).

[20] Yunfan Lu, Zipeng Wang, Minjie Liu, Hongjian Wang, and Lin Wang. 2023. Learning Spatial-Temporal Implicit Neural Representations for Event-Guided Video Super-Resolution. In *Proceedings of the IEEE/CVF Conference on Computer Vision and Pattern Recognition*. 1557–1567.

[21] Feifan Lv, Feng Lu, Jianhua Wu, and Chongsoon Lim. 2018. MBLLEN: Low-Light Image/Video Enhancement Using CNNs.. In *BMVC*, Vol. 220. 4.

[22] Chao Ma, Chih-Yuan Yang, Xiaokang Yang, and Ming-Hsuan Yang. 2017. Learning a no-reference quality metric for single-image super-resolution. *Computer Vision and Image Understanding* 158 (2017), 1–16.

[23] Long Ma, Tengyu Ma, Risheng Liu, Xin Fan, and Zhongxuan Luo. 2022. Toward fast, flexible, and robust low-light image enhancement. In *Proceedings of the IEEE/CVF Conference on Computer Vision and Pattern Recognition*. 5637–5646.

[24] Anish Mittal, Rajiv Soundararajan, and Alan C Bovik. 2012. Making a "completely blind" image quality analyzer. *IEEE Signal processing letters* 20, 3 (2012), 209–212.

[25] Mohammad Mostafavi, Lin Wang, and Kuk-Jin Yoon. 2021. Learning to reconstruct hdr images from events, with applications to depth and flow prediction. *International Journal of Computer Vision* 129 (2021), 900–920.

[26] Stefano Pini, Guido Borghi, and Roberto Vezzani. 2018. Learn to see by events: Color frame synthesis from event and rgb cameras. *arXiv preprint arXiv:1812.02041* (2018).

[27] Henri Rebecq, Daniel Gehrig, and Davide Scaramuzza. 2018. ESIM: an open event camera simulator. In *Conference on robot learning*. PMLR, 969–982.

[28] Olaf Ronneberger, Philipp Fischer, and Thomas Brox. 2015. U-net: Convolutional networks for biomedical image segmentation. In *Medical Image Computing and Computer-Assisted Intervention–MICCAI 2015: 18th International Conference, Munich, Germany, October 5-9, 2015, Proceedings, Part III 18*. Springer, 234–241.

[29] Lei Sun, Christos Sakaridis, Jingyun Liang, Qi Jiang, Kailun Yang, Peng Sun, Yaozu Ye, Kaiwei Wang, and Luc Van Gool. 2022. Event-based fusion for motion deblurring with cross-modal attention. In *European Conference on Computer Vision*. Springer, 412–428.

[30] Lei Sun, Christos Sakaridis, Jingyun Liang, Peng Sun, Jiezhang Cao, Kai Zhang, Qi Jiang, Kaiwei Wang, and Luc Van Gool. 2023. Event-Based Frame Interpolation with Ad-hoc Deblurring. In *Proceedings of the IEEE/CVF Conference on Computer Vision and Pattern Recognition*. 18043–18052.

[31] Stepan Tulyakov, Daniel Gehrig, Stamatios Georgoulis, Julius Erbach, Mathias Gehrig, Yuanyou Li, and Davide Scaramuzza. 2021. Time lens: Event-based video frame interpolation. In *Proceedings of the IEEE/CVF conference on computer vision and pattern recognition*. 16155–16164.

[32] N Venkatanath, D Praneeth, Maruthi Chandrasekhar Bh, Sumohana S Channappayya, and Swarup S Medasani. 2015. Blind image quality evaluation using perception based features. In *2015 twenty first national conference on communications (NCC)*. IEEE, 1–6.

[33] Bishan Wang, Jingwei He, Lei Yu, Gui-Song Xia, and Wen Yang. 2020. Event enhanced high-quality image recovery. In *Computer Vision–ECCV 2020: 16th European Conference, Glasgow, UK, August 23–28, 2020, Proceedings, Part XIII 16*. Springer, 155–171.

[34] Ruixing Wang, Xiaogang Xu, Chi-Wing Fu, Jiangbo Lu, Bei Yu, and Jiaya Jia. 2021. Seeing dynamic scene in the dark: A high-quality video dataset with mechatronic alignment. In *Proceedings of the IEEE/CVF International Conference on Computer Vision*. 9700–9709.

[35] Zhou Wang, Alan C Bovik, Hamid R Sheikh, and Eero P Simoncelli. 2004. Image quality assessment: from error visibility to structural similarity. *IEEE transactions on image processing* 13, 4 (2004), 600–612.

[36] Fang Xu, Lei Yu, Bishan Wang, Wen Yang, Gui-Song Xia, Xu Jia, Zhendong Qiao, and Jianzhuang Liu. 2021. Motion deblurring with real events. In *Proceedings of the IEEE/CVF International Conference on Computer Vision*. 2583–2592.

[37] Xiaogang Xu, Ruixing Wang, Chi-Wing Fu, and Jiaya Jia. 2022. SNR-aware low-light image enhancement. In *Proceedings of the IEEE/CVF conference on computer vision and pattern recognition*. 17714–17724.

[38] Shuzhou Yang, Moxuan Ding, Yanmin Wu, Zihan Li, and Jian Zhang. 2023. Implicit neural representation for cooperative low-light image enhancement. In *Proceedings of the IEEE/CVF International Conference on Computer Vision*. 12918–12927.

[39] Yixin Yang, Jin Han, Jinxiu Liang, Imari Sato, and Boxin Shi. 2023. Learning event guided high dynamic range video reconstruction. In *Proceedings of the IEEE/CVF Conference on Computer Vision and Pattern Recognition*. 13924–13934.

[40] Fan Zhang, Yu Li, Shaodi You, and Ying Fu. 2021. Learning temporal consistency for low light video enhancement from single images. In *Proceedings of the IEEE/CVF conference on computer vision and pattern recognition*. 4967–4976.

[41] Lin Zhang, Lei Zhang, and Alan C Bovik. 2015. A feature-enriched completely blind image quality evaluator. *IEEE Transactions on Image Processing* 24, 8 (2015), 2579–2591.

[42] Richard Zhang, Phillip Isola, Alexei A Efros, Eli Shechtman, and Oliver Wang. 2018. The unreasonable effectiveness of deep features as a perceptual metric. In *Proceedings of the IEEE conference on computer vision and pattern recognition*. 586–595.

[43] Shen Zheng and Gaurav Gupta. 2022. Semantic-guided zero-shot learning for low-light image/video enhancement. In *Proceedings of the IEEE/CVF Winter conference on applications of computer vision*. 581–590.

[44] Alex Zihao Zhu, Liangzhe Yuan, Kenneth Chaney, and Kostas Daniilidis. 2019. Unsupervised event-based learning of optical flow, depth, and egomotion. In *Proceedings of the IEEE/CVF Conference on Computer Vision and Pattern Recognition*. 989–997.